JAMES | Journal of Advances in Modeling Earth Systems

RESEARCH ARTICLE
10.1029/2021MS002922

The Two-Energies Turbulence Scheme Coupled to the Assumed PDF Method

Ivan Bašták Ďurán[1,2], **Mirjana Sakradzija**[2,3], **and Juerg Schmidli**[1,2]

[1]Institute for Atmospheric and Environmental Sciences, Goethe University Frankfurt, Frankfurt am Main, Germany, [2]Hans Ertel Centre for Weather Research, Offenbach am Main, Germany, [3]Deutscher Wetterdienst, Offenbach am Main, Germany

Key Points:

- An update of the two-energy scheme for the unified parameterization of the turbulence and clouds in the atmospheric boundary layer (ABL) is presented
- The performance of the updated scheme is comparable to the operational ICOsahedral Nonhydrostatic configuration
- The updated scheme shows the ability to model coherent flow structures in the ABL

Correspondence to:
I. Bašták Ďurán,
bastakdu@iau.uni-frankfurt.de

Citation:
Bašták Ďurán, I., Sakradzija, M., & Schmidli, J. (2022). The two-energies turbulence scheme coupled to the assumed PDF method. *Journal of Advances in Modeling Earth Systems*, *14*, e2021MS002922. https://doi.org/10.1029/2021MS002922

Received 27 NOV 2021
Accepted 30 APR 2022

Author Contributions:
Conceptualization: Ivan Bašták Ďurán, Mirjana Sakradzija, Juerg Schmidli
Data curation: Ivan Bašták Ďurán, Mirjana Sakradzija, Juerg Schmidli
Formal analysis: Ivan Bašták Ďurán, Mirjana Sakradzija, Juerg Schmidli
Funding acquisition: Ivan Bašták Ďurán, Juerg Schmidli
Investigation: Ivan Bašták Ďurán, Mirjana Sakradzija, Juerg Schmidli
Methodology: Ivan Bašták Ďurán, Mirjana Sakradzija, Juerg Schmidli
Project Administration: Ivan Bašták Ďurán, Mirjana Sakradzija, Juerg Schmidli
Resources: Ivan Bašták Ďurán, Mirjana Sakradzija, Juerg Schmidli

Abstract An update of the two-energy turbulence scheme is presented, the 2TE + APDF scheme. The original version of the two-energy scheme is able to successfully model shallow convection without the need of an additional parameterization for non-local fluxes. However, the performance of the two-energy scheme is worse in stratocumulus cases, where it tends to overestimate the erosion of the stable layers. We have identified the causes: the non-local stability parameter does not consider local stratification, the scheme lacks an internal parameter that could distinguish between a shallow convection regime and a stratocumulus regime, and it uses an inflexible turbulence length scale formulation. To alleviate this problem, we propose several modifications: an update of the stability parameter, a modified computation of the turbulence length scale, and the introduction of the entropy potential temperature to distinguish between a shallow convection and a stratocumulus regime. In addition, the two-energy scheme is coupled to a simplified assumed probability density function method in order to achieve a more universal representation of the cloudy regimes. The updated turbulence scheme is evaluated for several idealized cases and one selected real case in the ICOsahedral Nonhydrostatic (ICON) modeling framework. The results show that the updated scheme corrects the overmixing problem in the stratocumulus cases. The performance of the updated scheme is comparable to the operational setup, and can be thus used instead of the operational turbulence and shallow convection scheme in ICON. Additionally, the updated scheme improves the coupling with dynamics, which is beneficial for the modeling of coherent flow structures in the atmospheric boundary layer.

Plain Language Summary The two-energy turbulence scheme parametrizes turbulence and boundary layer clouds in a unified framework. This enables the scheme to be more consistent and more continuous in time and space than the classical combination of separate turbulence and convection schemes. The original version of the scheme tends to overestimate the erosion of the stable layers, particularly in stratocumulus cases. We have identified several reasons for this problem and updated the scheme accordingly. To achieve a more universal representation of the cloudy regimes, the two-energy scheme has been also coupled to the assumed probability density function (PDF) method. This method is based on assuming the shape of the trivariate PDF of moisture, heat and vertical velocity. The new version of the scheme was implemented into the ICOsahedral Nonhydrostatic (ICON) modeling framework and was tested on several idealized cases and one realistic case. The results show that the updated scheme corrects the overmixing problem in the stratocumulus cases. The performance of the updated scheme is comparable to the operational setup, and can be thus used instead of the operational turbulence and shallow convection scheme in ICON. Additionally, the updated scheme improves the coupling with dynamics, which is beneficial for the modeling of coherent flow structures in the atmospheric boundary layer.

1. Introduction

In previous papers (Bašták Ďurán et al., 2014, 2018) the authors derived a turbulence scheme based on two prognostic turbulence energies with the aim to parameterize turbulence and clouds in the atmospheric boundary layer (ABL) in a unified way.

The two-energy (2TE) approach originates in the work of S. S. Zilitinkevich et al. (2007) and S. Zilitinkevich et al. (2008, 2013), who proposed the usage of two turbulence energies in the stable boundary layer. In Bašták Ďurán et al. (2018), this work is extended to all atmospheric stabilities in the framework of Bašták Ďurán et al. (2014). The influence of moisture on turbulence mixing is also accounted for. The fundamental difference between the two-energy scheme and turbulence schemes with only one prognostic turbulence energy, the

Software: Ivan Bašták Ďurán, Mirjana Sakradzija, Juerg Schmidli
Validation: Ivan Bašták Ďurán, Mirjana Sakradzija, Juerg Schmidli
Visualization: Ivan Bašták Ďurán, Mirjana Sakradzija, Juerg Schmidli
Writing – original draft: Ivan Bašták Ďurán, Mirjana Sakradzija, Juerg Schmidli
Writing – review & editing: Ivan Bašták Ďurán, Mirjana Sakradzija, Juerg Schmidli

turbulence kinetic energy (TKE), is in the computation of the stability parameter. While in TKE schemes (e.g., Cheng et al., 2002; Cuxart et al., 2000; Doms et al., 2018; Janjic, 2002), the stability parameter is computed only locally and diagnostically (e.g., gradient Richardson number, *Ri*), the stability parameter in the two-energy scheme is computed from the prognostic energies and is thus independent from local gradients and has a prognostic character. A similar behavior was achieved in Bretherton and Park (2009) by extending their convective layers into stable regions and merging them if they overlap and by using averaged stability functions across each of these layers. The non-local and prognostic properties of the stability parameter lead to deeper mixing and transport across locally stable layers, which enables the two-energy scheme to model both turbulence and shallow convection (cloud depth is smaller than a prescribed value; see Sakradzija et al. (2020)) without an additional parameterization for non-local fluxes.

This is in contrast with the traditional separation of these processes into a local down-gradient parameterization (the turbulent fluxes are proportional to the local gradients) and a non-local parameterization (A. A. M. Holtslag & Moeng, 1991; Bechtold et al., 2001, 2014; Deardorff, 1972; Neggers, 2009; Neggers et al., 2009; Siebesma et al., 2007; Sušelj et al., 2012; Tiedtke, 1989), which complements the local mixing with transport caused by thermals. Even though such a separation of processes is more transparent and can be better controlled than a unified scheme, it can also introduce problems with compensating errors, and complicates the representation of interactions and transitions. Regarding these issues, the separation of the processes can be also avoided by using turbulence schemes with a Higher Order turbulence Closure (HOC), where the higher order moments enable the representation of non-local and counter-gradient transport (Bougeault, 1981; Golaz et al., 2002; Krueger, 1988; Machulskaya & Mironov, 2013; Nakanishi & Niino, 2009). Compared to the two-energy scheme, the HOC schemes are more sophisticated and require thus shorter time steps due to numerical stability constraints, which makes them computationally more expensive.

It has been shown in Bašták Ďurán et al. (2018) that the two energy scheme can successfully model shallow convection. However, the performance of the two-energy scheme is worse in stratocumulus cases, where it tends to overestimate the erosion of the stable layers (particularly at the top of the ABL) due to overmixing. To alleviate this problem, we update the computation of the stability parameter and of the turbulence length scale, and make the vertical TKE transport dependent on the entropy potential temperature (Marquet, 2011).

A critical factor in the parameterization of ABL clouds is the influence of moisture and phase changes of water on turbulence mixing. In the two-energy scheme, this effect is represented through the influence of moisture (latent heat and changes in density) on the buoyancy term in the TKE equation. In the original scheme, the buoyancy term is expressed as a linear combination of co-variances for liquid water potential temperature and total specific water content according to Sommeria and Deardorff (1977) and Marquet and Geleyn (2013) with a skewness dependent heuristic adjustment. This heuristic approach is successful for modeling of the shallow convection regime, but lacks the universality to be used in all possible regimes in the ABL (e.g., stratocumulus cases and transition regimes).

Therefore, we couple the two-energy scheme to a simplified assumed probability density function (APDF) method (Bogenschutz & Krueger, 2013; Golaz et al., 2002; V. Larson et al., 2012; V. E. Larson et al., 2002), which offers a more universal representation of cloudy regimes. The APDF method is based on the assumed shape of the joint trivariate probability density function (PDF) of temperature, moisture and vertical velocity. Cloud related quantities, such as the buoyancy flux, are then computed in a consistent way from the joint PDF. The key parameter in the estimation of the joint PDF is the vertical velocity skewness. The later is also related to the vertical transport of turbulence energies in their prognostic equations. We thus parameterize the vertical velocity skewness and the two vertical transport terms consistently with the same down-gradient closure.

A version of the two-energy scheme is used operationally in the ALADIN NWP model within the ALARO physical package (Termonia et al., 2018; Wang et al., 2018) and is implemented in the Integrated Forecast System model developed at the European Centre for Medium-Range Weather Forecasts. In the present paper, the coupled 2TE + APDF scheme is tested within the ICON (ICOsahedral Nonhydrostatic) modeling framework (Crueger et al., 2018; Dipankar et al., 2015; Giorgetta et al., 2018; Heinze et al., 2017; Zängl et al., 2015).

This paper is organized as follows. Section 2 gives a general overview of our proposal to couple the two-energy scheme to the APDF method with additional updates to the computation of the stability parameter and the turbulence length scale. The scheme is evaluated in Section 3 for idealized cases in the single column mode (SCM) and

the cloud resolving mode (CRM; Bašták Ďurán et al., 2021) of the ICON model, and for a real-case simulation in Section 4. We finish with a summary and conclusions in Section 5.

2. The 2TE Scheme Coupled to the APDF Method

2.1. The 2TE Scheme

We start by summarizing the key properties of the original 2TE scheme (Bašták Ďurán et al., 2018).

The turbulent fluxes in the 2TE scheme are parameterized using a down-gradient closure:

$$\overline{u'w'} = -K_M \frac{\partial u}{\partial z}, \quad \overline{v'w'} = -K_M \frac{\partial v}{\partial z}, \tag{1}$$

$$\overline{\theta_l' w'} = -K_H \frac{\partial \theta_l}{\partial z}, \quad \overline{q_t' w'} = -K_H \frac{\partial q_t}{\partial z} \tag{2}$$

$$K_M = C_K \, L \, \chi_3 \left(Ri_f\right) . \sqrt{e_k}, \tag{3}$$

$$K_H = C_3 \, C_K \, L \, \phi_3 \left(Ri_f\right) . \sqrt{e_k}, \tag{4}$$

where u, v, and w are the wind components, θ_l is the liquid water potential temperature, q_t is total specific water content, z is the height, K_M and K_H are the exchange coefficients for momentum and heat, L is the turbulence length scale, e_k is the TKE, χ_3 and ϕ_3 are stability functions for momentum and heat with:

$$Ri_f \equiv -\frac{B}{S}, \tag{5}$$

$$S = -\overline{u'w'} \frac{\partial u}{\partial z} - \overline{v'w'} \frac{\partial v}{\partial z}, \tag{6}$$

$$B = \frac{g}{\rho_0} \overline{w'\rho'} \approx E_{\theta_l} \, \overline{w'\theta_l'} + E_{q_t} \, \overline{w'q_t'}, \tag{7}$$

where Ri_f is the flux Richardson number, S and B are the shear production term and the buoyancy production/destruction term in the prognostic turbulence equations, g is the gravitational acceleration, ρ is air density, and ρ_0 is the reference air density, E_{θ_l} and E_{q_t} are weights computed from the sub-grid-scale cloud fraction, C_{sgr}, according to Marquet and Geleyn (2013) with a skewness dependent heuristic adjustment (see Bašták Ďurán et al., 2018), C_3 is the inverse of the Prandtl number at neutrality, and C_K (see Cheng et al., 2002) is a closure constant. C_{sgr} is estimated by using the Gaussian formulation of Sommeria and Deardorff (1977).

The prognostic equations for the turbulence energies are used in the following form:

$$\frac{de_k}{dt} = \frac{\partial}{\partial z} \left(K_{e_k} \frac{\partial e_k}{\partial z} \right) + S + B - \frac{2\, e_k}{\tau_k}, \tag{8}$$

$$\frac{de_s}{dt} = \frac{\partial}{\partial z} \left(K_{e_s} \frac{\partial e_s}{\partial z} \right) + S - \frac{2\, e_s}{\tau_s}, \tag{9}$$

$$e_k \equiv 0.5 \left(\overline{u'^2} + \overline{v'^2} + \overline{w'^2} \right), \tag{10}$$

$$e_s \equiv e_k + E_{q_t} \frac{\overline{q_t'^2}}{2 \frac{\partial q_t}{\partial z}} + E_{\theta_l} \frac{\overline{\theta_l'^2}}{2 \frac{\partial \theta_l}{\partial z}}, \tag{11}$$

$$\tau_k = \frac{2\, L}{C_\epsilon \sqrt{e_k}}, \tag{12}$$

$$\tau_s \equiv \left[\left(\frac{C_4}{2\, C_3} - 1 \right) Ri_f^{TE} + 1 \right] \tau_k \tag{13}$$

$$Ri_f^{TE} = \frac{e_s - e_k}{e_s + e_k\left(\frac{C_4}{2C_3} - 1\right)}, \tag{14}$$

$$K_{e_k} = K_{e_s} = C_{e_k}\overline{w'^2}\tau_k, \tag{15}$$

where e_s is the second prognostic energy, τ_k and τ_s are the dissipation time scales for e_k and e_s, Ri_f^{TE} is an estimate of Ri_f (see Bašták Ďurán et al., 2018), based on the two prognostic energies, C_4, $C_{e_k} = 0.1$, and C_ϵ are closure constants; and K_{e_k} and K_{e_s} are the turbulent diffusion coefficients for e_k and e_s. For the sake of simplicity it is assumed that $K_{e_s} = K_{e_k}$.

The χ_3 and ϕ_3 stability functions are then computed using the Ri_f^{TE} estimate of the flux Richardson number:

$$\phi_3\left(Ri_f^{TE}\right) = \frac{1 - Ri_f^{TE}/P}{1 - Ri_f^{TE}}, \tag{16}$$

$$\chi_3\left(Ri_f^{TE}\right) = \frac{1 - Ri_f^{TE}/R}{1 - Ri_f^{TE}}, \tag{17}$$

where P and R are either constants or functions of Ri_f depending on the complexity of the chosen scheme (for details, see Bašták Ďurán et al. (2014)). In this paper we use $P = 0.367$ and $R = 0.334$.

The turbulence length scale is computed as a combination of two length scale formulations:

$$L = \min\left(L_1, L_2\right), \tag{18}$$

where L_1 is computed from the ABL height, H_{abl} (Cedilnik, 2005):

$$L_1 = \frac{\left(C_K\, C_\epsilon\right)^{\frac{1}{4}}}{C_K} \frac{\kappa z}{1 + \frac{\kappa z}{\lambda_m}\left[\frac{1 + \exp\left(-a_m\sqrt{\frac{z}{H_{\text{abl}}}} + b_m\right)}{\beta_m + \exp\left(-a_m\sqrt{\frac{z}{H_{\text{abl}}}} + b_m\right)}\right]} \tag{19}$$

and L_2 is given by balance between TKE and local stability (Bougeault & Lacarrere, 1989):

$$L_2 = \left(\frac{L_{\text{up}}^{-\frac{4}{5}} + L_{\text{down}}^{-\frac{4}{5}}}{2}\right)^{-\frac{5}{4}}. \tag{20}$$

κ is the von Kármán constant; $a_m = 7.5$, $b_m = 3.0$, $\beta_m = 0.11$, and $\lambda_m = 350$ are constants; and L_{up} and L_{down} are the upward and the downward free paths.

2.1.1. Issues With the Original 2TE Scheme

The 2TE scheme works well for shallow convection cases, however it tends to overestimate the erosion of stable layers due to overmixing, which influences the performance of the scheme particularly in stratocumulus cases. We have identified the causes of the overmixing in stable layers in the original version of the scheme. First, the non-local stability parameter did not consider local stratification, which lead to its underestimation and subsequent overmixing. Second, the scheme lacked an internal parameter that could distinguish between a shallow convection and a stratocumulus regime, thus the scheme could not be calibrated in this respect. And third, the turbulence length scale formulation was not flexible enough to adjust to all possible regimes in the ABL.

2.2. Update of the 2TE Scheme

2.2.1. The Stability Parameter

In order to re-introduce the effect of the local stratification into the 2TE scheme, the stability parameter is computed as a combination of a non-local and a local estimation of the flux Richardson number:

$$Ri_f^* = C_{Ri_f}\, Ri_f^{GR} + \left(1 - C_{Ri_f}\right)\, Ri_f^{TE} \tag{21}$$

where Ri_f^{TE} is the non-local estimate computed from the prognostic energies (see Equation 14) and

$$Ri_f^{GR} = \frac{K_H\left(Ri_f^{GR}\right)}{K_M\left(Ri_f^{GR}\right)} Ri = \frac{C_3 R\left(P - Ri_f^{GR}\right)}{R\left(P - Ri_f^{GR}\right)} Ri \tag{22}$$

is the local estimate calculation from local gradients, where Ri is the gradient Richardson number, and $C_{Ri_f} = 0.8$ is a calibration constant. Ri_f^* is used instead of Ri_f^{TE} in the calculation of the χ_3 and ϕ_3 stability functions in Equations 16 and 17.

2.2.2. The Entropy Potential Temperature

Recently, it has been shown that the entropy potential temperature, θ_s, (potential temperature that has the same conservative properties as the moist entropy; see Marquet (2011) and Marquet and Geleyn (2013)) can be used to distinguish between the shallow convection regime and the stratocumulus regime (Marquet & Bechtold, 2020; Marquet & Stevens, 2021).

We exploit this fact by making the vertical exchange coefficient for turbulence energies dependent on the vertical flux of the entropy potential temperature, $\overline{w'\theta_s'}$. The extension is made by using the expression for $\overline{w'^3}$ according to the A_1 part of Equations 14a and 14d in Canuto et al. (2007), where we replace the potential heat flux with $\overline{w'\theta_s'}$:

$$K_{e_k} = K_{e_s} = \left(C_{\overline{w'^2}}\overline{w'^2} + C_{\theta_s}\frac{g}{\theta_0}\overline{w'\theta_s'}\tau_k\right)\tau_k, \tag{23}$$

$$\overline{w'\theta_s'} = (1 + \Lambda q_t)\,\overline{w'\theta_l'} + \Lambda\,\theta_s\overline{w'q_t'} \tag{24}$$

$$\theta_s = \theta_l \exp\left(\Lambda\, q_t\right) \tag{25}$$

where θ_0 is the reference potential temperature, $C_{\overline{w'^2}}$ and C_{θ_s} are calibration constants, and $\Lambda = 5.87$ is a closure constant. Thanks to the dependence on $\overline{w'\theta_s'}$, the vertical transport of the turbulence energies is stronger in the shallow convection cases and weaker in the stratocumulus cases.

2.2.3. The Turbulence Length Scale

To make the turbulence length scale more flexible and at the same time more continuous in time and space, we compute the turbulence length scale from the ABL height according to Equation 19 (with modified calibration constants: $a_m = 10.0$, $b_m = 4.5$, and $\lambda_m = 600$):

$$L = \frac{\frac{\left(C_K\, C_e\right)^{\frac{1}{4}}}{C_K}\kappa z}{1 + \frac{\kappa z}{\lambda_m}\left[\frac{1+\exp\left(-a_m\sqrt{\frac{z}{H_{\mathrm{abl}}}}+b_m\right)}{\beta_m+\exp\left(-a_m\sqrt{\frac{z}{H_{\mathrm{abl}}}}+b_m\right)}\right]}. \tag{26}$$

The ABL height is estimated from the balance between TKE and local stability (Bougeault & Lacarrere, 1989). More specifically, the ABL height is dependent on the vertical integral of the upward free path, L_{up}:

$$H_{\mathrm{abl}} = C_{ablh}\int_z L_{up}\,dz, \tag{27}$$

where $C_{ablh} = 1.75$ is a calibration constant.

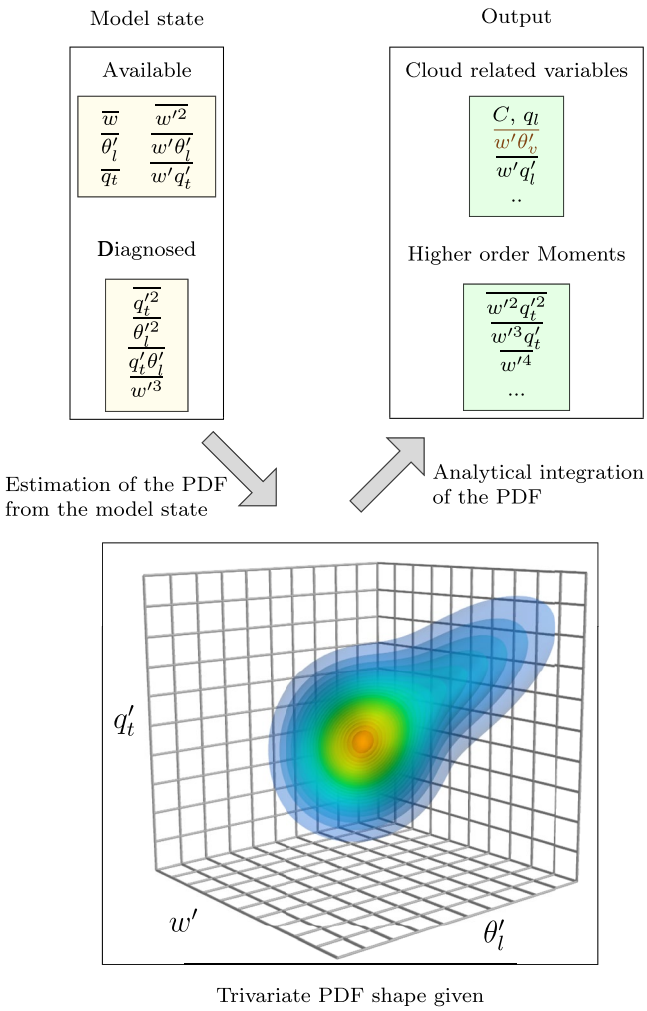

Figure 1. Schematics of the assumed probability density function (APDF) method. In the coupled 2TE + APDF scheme, only the outputted flux of the virtual potential temperature, $\overline{w'\theta'_v}$, is actively used.

Following results from Bašták Ďurán et al. (2020), the asymptotic behavior in the free atmosphere of the turbulence length scale is also adjusted. The β_m parameter is dependent on the bulk gradient of the entropy potential temperature in the lower part of the atmosphere:

$$\Delta\theta_s \le C_{\beta_m} \;:\; \beta_m = \beta_m^u, \tag{28}$$

$$\left(\Delta\theta_s \ge C_{\beta_m}\right) \,\&\, \left(\Delta\theta_s \le -C_{\beta_m}\right) \;:\; \beta_m = \frac{\beta_m^u}{2}\left(1 - \frac{\Delta\theta_s}{C_{\beta_m}}\right), \tag{29}$$

$$\Delta\theta_s > C_{\beta_m} \;:\; \beta_m = 0, \tag{30}$$

$$\Delta\theta_s = \theta_s\left(z = 1.5H_{\text{abl}}\right) - \theta_s\left(z = 0\right) \tag{31}$$

where $\beta_m^u = 0.07$ and $C_{\beta_m} = 0.005$ is a calibration constant. In this way the turbulence length scale converges in the free atmosphere to zero in the stable cases and stratocumulus cases and to a non-zero asymptotic value in the shallow convection cases.

2.3. Coupling of the 2TE Scheme With the APDF Method

The core of the APDF method is a joint trivariate PDF (w, θ_l, and q_t), which is used to close the Reynolds-averaged Navier-Stokes equations by computing the higher order moments and buoyancy terms via analytic integration of the PDF. To keep our turbulence scheme relatively simple, we don't use the whole potential of the APDF method and employ it only for the computation of the buoyancy source term in the TKE equation (similarly to Bogenschutz and Krueger (2013)). The internal cloud fraction of the APDF method can be used for further diagnostics.

The joint PDF is a simplified double Gaussian (for details, see Golaz et al. (2002)):

$$\begin{aligned} P_{APDF}\left(w, \theta_l, q_t\right) = a\, G_1\left(w, \theta_l, q_t\right) + \\ (1-a) G_2\left(w, \theta_l, q_t\right), \end{aligned} \tag{32}$$

where G_1 and G_2 are individual trivariate Gaussians. The above PDF has 10 free parameters: the relative weight of the first Gaussian, a, the locations and the widths of the w, θ_l, and q_t Gaussians; and the intra-Gaussian correlation between θ_l and q_t. The free parameters need to be determined at each location and time step from the model state, which is characterized by the mean values of w, θ_l, and q_t, their second order moments, and the skewness of vertical velocity.

In our coupled simplified implementation, the mean values $\overline{w}$, $\overline{\theta_l}$ and $\overline{q_t}$; and the turbulent fluxes $\overline{w'\theta'_l}$, $\overline{w'q'_t}$, and $\overline{w'^2}$ are available from the two-energy scheme, but the remaining second order moments and the third order moment of the vertical velocity need to be diagnosed (see Figure 1 for an illustration of the coupling). For the former, we use the diagnostic form of the equations for the second order moments (see, e.g., Equations 36–38 in Bašták Ďurán et al. (2018)):

$$\frac{\overline{q'_t\theta'_l}}{\tau_k \frac{C_4}{2C_3}} = -\frac{\partial\theta_l}{\partial z}\overline{w'q'_t} - \frac{\partial q_t}{\partial z}\overline{w'\theta'_l}, \tag{33}$$

$$\frac{2\overline{q'^2_t}}{\tau_k \frac{C_4}{2C_3}} = -\frac{\partial q_t}{\partial z}\overline{w'q'_t}, \tag{34}$$

$$\frac{2\overline{\theta_l'^2}}{\tau_k \frac{C_4}{2C_3}} = -\frac{\partial \theta_l}{\partial z}\overline{w'\theta_l'} \tag{35}$$

and the third order moment of the vertical velocity is estimated using a down-gradient closure, consistent with the expression for the turbulent transport of e_k and e_s:

$$\overline{w'^3} = -K_{e_k}\frac{\partial \overline{w'^2}}{\partial z}. \tag{36}$$

The coupling of the 2TE scheme to the APDF method is then finalized by using the buoyancy source term obtained from the trivariate PDF (see Figure 1) in the TKE equation:

$$B = \frac{g}{\theta_0}\overline{w'\theta_v'}, \tag{37}$$

$$\overline{w'\theta_v'} = \overline{w'\theta_l'} + \frac{1-\epsilon_0}{\epsilon_0}\theta_0\overline{w'q_t'} + \left[\frac{L_v}{c_p}\left(\frac{p_0}{p}\right)^{\frac{R_d}{c_p}} - \frac{\theta_0}{\epsilon_0}\right]\overline{w'q_l'}, \tag{38}$$

where the vertical turbulent flux of the liquid water content, $\overline{w'q_l'}$, is computed from the trivariate PDF according to Equation A13 in V. E. Larson et al. (2002).

3. Idealized Simulations

To evaluate our turbulence scheme we implemented it into the ICON modeling system. The ICON model is a fully compressible model that performs computations in grid-point space on geodesic Delaunay grids with C-type staggering (Zängl et al., 2015). A comprehensive description of the ICON model can be found in the referenced articles. For the sake of brevity, we will not give an in-depth introduction of the ICON model. We only highlight that the local down-gradient turbulent mixing is parameterized via a TKE closure scheme (Cerenzia, 2017; Doms et al., 2013) and that the convection scheme for both shallow and deep convection is based on a mass-flux scheme, where the entrainment and detrainment include contributions from turbulent and organized parts (Bechtold et al., 2008).

The 2TE + APDF scheme was first tested on four idealized cases, all developed by the Global Energy and Water Cycle Experiment (GEWEX): the drizzling stratocumulus case based on the first research flight (RF01) of the second Dynamics and Chemistry of Marine Stratocumulus (DYCOMS-II) field study (Stevens et al., 2005), the continental cumulus case based on measurements over the Atmospheric Radiation Measurement (ARM) program Cloud and Radiation Testbed (CART) site in Oklahoma (Brown et al., 2002; Lenderink et al., 2004), the trade wind cumulus case based on observations from the Barbados Oceanographic and Meteorological Experiment (BOMEX; Siebesma et al., 2003), and the fourth test case is based on the GEWEX Atmospheric Boundary Layer Study (GABLS1) project (Beare et al., 2006; B. Holtslag, 2006; Cuxart et al., 2006). This particular set of cases was chosen to evaluate the skill of the 2TE + APDF scheme to handle regimes with clouds in the ABL: shallow convection (ARM and BOMEX) and stratocumulus (DYCOMS-II). The weakly stable case (GABLS1) should verify whether the 2TE + APDF scheme is useable also in stable conditions.

The idealized cases were tested on the SCM and CRM configuration of ICON (Bašták Ďurán et al., 2021). The SCM configuration basically runs on a single column with deactivated dynamics. The CRM configuration is forced identically to the SCM (same boundary conditions and atmospheric forcings), but runs with activated dynamics in 3D on a 100 × 100 torus grid with grid spacing of 5 km. The SCM was chosen to analyze the impact of physical parameterization on the model performance without interaction with dynamics. The CRM includes the interactions with dynamics, but the large scale forcings and boundary conditions are still idealized. All SCM simulations are performed with a 5 s time step, and the same vertical grid as used for the operational numerical weather forecasts, with 90 atmospheric levels, the model top at 75 km and 14 levels in the lowest 2 km.

Table 1
Horizontal (l_x and l_y) and Vertical Domain Size (l_z), Horizontal (Δl_{xy}) and Vertical Resolution (Δl_z), and Integration Time (T_{int}) for the Large Eddy Simulation Runs

Case	$l_x \times l_y$ (km × km)	Δl_{xy} (m)	l_z (m)	Δl_z (m)	T_{int} (hr)
ARM	6.4 × 6.4	100	4,400	34.75	14
BOMEX	6.4 × 6.4	100	3,000	46.875	16
DYCOMS-II	4.096 × 4.096	32	1,500	11.71875	16
GABLS1	0.4 × 0.4	3.125	400	3.125	9

In our experiments, we use two sets of physical parameterization setups: the NWP setup—the ICON setup according to the operational model version that is valid since 14 April 2021 (Zängl & Schäfer, 2021) and the 2TE + APDF setup—same as the NWP setup, but the NWP atmospheric turbulence and convection parameterizations are deactivated and replaced with the 2TE + APDF scheme. Our goal here is to show that 2TE + APDF scheme is able to replace both turbulence and convection parameterization in selected cases.

The SCM and CRM results for the above cases were compared with results from the large eddy simulation (LES) model MicroHH (C. van Heerwaarden et al., 2017; C. C. van Heerwaarden et al., 2017). In the ARM, BOMEX, and DYCOMS-II simulation MicroHH runs with moist thermodynamics and in the GABLS simulation with dry thermodynamics. Parameterization of radiation and microphysics was used only in the DYCOMS-II case. These processes were deactivated in the remaining cases. The setups of the idealized cases follow the recommendation in their respective inter-comparison studies and are summarized in Table 1. The LES statistics were averaged over the whole horizontal domain in space and over 1 hr in time.

Figure 2 shows the vertical profiles of the horizontal wind speed, the liquid water potential temperature, θ_l, the total specific water content, q_t, and the cloud fraction, C, for the LES, the SCM and the CRM. The 2TE + APDF scheme shows a comparable overall performance to the ICON NWP setup. The NWP setup is however able to maintain sharper gradients, which is visible mainly in the wind profiles and for the DYCOMS-II case. The overmixing at the top of the ABL in stratocumulus cases was a pronounced problem in the original 2TE scheme (Bašták Ďurán et al., 2018). The 2TE + APDF scheme does not produce such sharp gradients as the NWP setup, but it is able to model the DYCOMS-II case in a realistic way (close to the LES reference). This is a significant improvement compared to the original 2TE scheme. The advantage of the 2TE + APDF scheme compared to the NWP setup is better (lower) ABL height in the GABLS1 case and it does not overmix (as the NWP setup) in the ARM and BOMEX cases. Both setups tend to overestimate the cloud fraction in the DYCOMS-II and the BOMEX cases. In the ARM case, the vertical extend of the cloud fraction is better (deeper) for the NWP setup, but the 2TE + APDF scheme has a better estimate near the cloud base.

Similar to the results with the 2TE scheme (Bašták Ďurán et al., 2018), the vertical profiles with the 2TE + APDF scheme are more continuous in space. This is particularly visible in the cloud fraction profiles. The NWP setup, which uses a mass-flux based scheme for the parameterization of convection, generates jagged profiles. This is a consequence of the on-off behavior of the mass-flux scheme (Bašták Ďurán et al., 2018) that is caused by the combination of the too fast mixing (immediate non-local mixing) and a relatively sensitive triggering mechanism in the convection scheme. The 2TE + APDF scheme is more continuous in space (and time), because its mixing is controlled via a pair of prognostic turbulence energies and not via a trigger mechanism.

These properties are even more visible in the evolution of the cloud fraction and TKE, which are presented in Figures 3 and 4. Since TKE is a measure of the turbulence mixing intensity, it is clear that the turbulent mixing in the NWP setup is influenced by the activity of the convection scheme. This results in bursts of turbulence mixing, which are not present in the LES reference. The 2TE + APDF scheme does not suffer from such behavior, because it is not linked to any convection scheme. Thanks to the unified parameterization of turbulence and convection in the ABL, the 2TE + APDF scheme has a closer coupling to the dynamics of the model when the dynamics is activated (see Section 4). The comparison between the SCM and the CRM shows, that the dynamics in the selected idealized cases increases the vertically transport. In general, this is beneficial for the NWP setup, which was calibrated to function together with the dynamics. The influence of dynamics on the vertical transport in the 2TE + APDF scheme is weaker, because the 2TE + APDF scheme does not generate such strong vertical gradients. The influence of the dynamics on the horizontal transport will be analyzed in Section 4.

In general, the results show that the 2TE + APDF scheme can be used instead of a combination of the operational turbulence and convection schemes. The advantage of the current 2TE + APDF scheme is in its more continuous behavior. It does, however, not have the ability to maintain such sharp gradients as the NWP setup and it also mixes slower and sometimes shallower than the mass-flux scheme. It is possible that calibration could mitigate these two disadvantages.

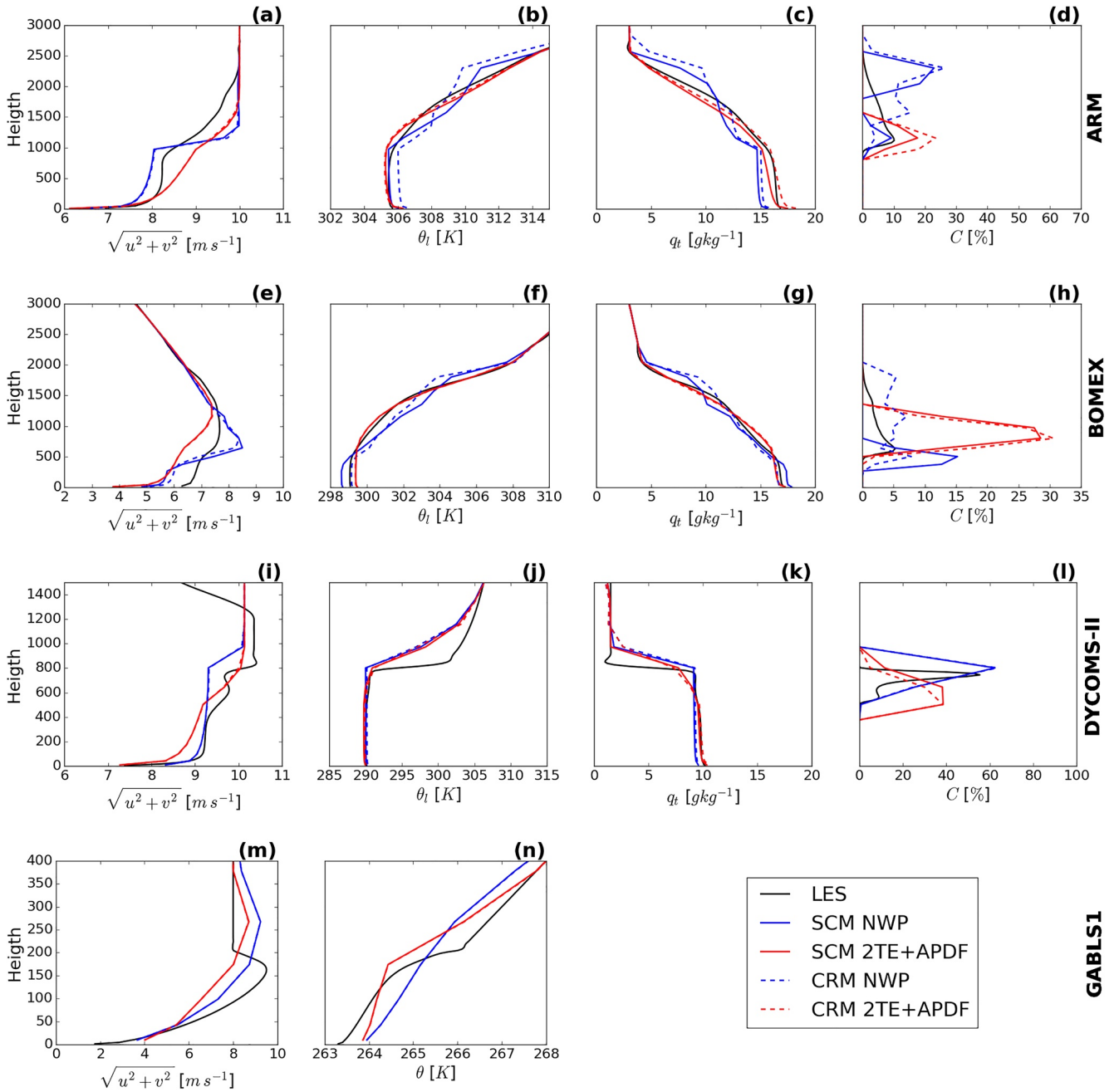

Figure 2. Vertical profiles of the horizontal wind speed (a, e, i, m), the liquid water potential temperature (b, f, j, n), the total specific content of water (c, g, k), and the cloud fraction (d, h, l) for Atmospheric Radiation Measurement (ARM), Barbados Oceanographic and Meteorological Experiment (BOMEX), Dynamics and Chemistry of Marine Stratocumulus (DYCOMS-II), and GEWEX Atmospheric Boundary Layer Study (GABLS1) cases after 8 hr of integration. Comparison between large eddy simulation (LES; black), ICOsahedral Nonhydrostatic single column mode (ICON SCM; solid line) and cloud resolving mode (CRM; dashed line) with operational setup (blue), and ICON SCM (solid line) and CRM (dashed line) with 2TE + APDF scheme (red).

The internal properties of the updated 2TE + APDF scheme are illustrated in Figure 5. The first column shows a comparison of the vertical profiles of the 2TE + APDF turbulence length scale (Equation 26) and the diagnosed 2TE turbulence length scale (Equation 18) in ICON SCM simulations. Clearly, the biggest difference is in the asymptotic values above the ABL top. The 2TE turbulence length scale converges always to zero thanks to the influence of the TKE based L_2 length scale. In comparison, the asymptotic values of the 2TE + APDF turbulence length scale is zero only for the stable GABLS1 case. It is larger for the DYCOMS-II stratocumulus case and is largest for the ARM and BOMEX shallow convection cases. This corresponds to the intended design of the

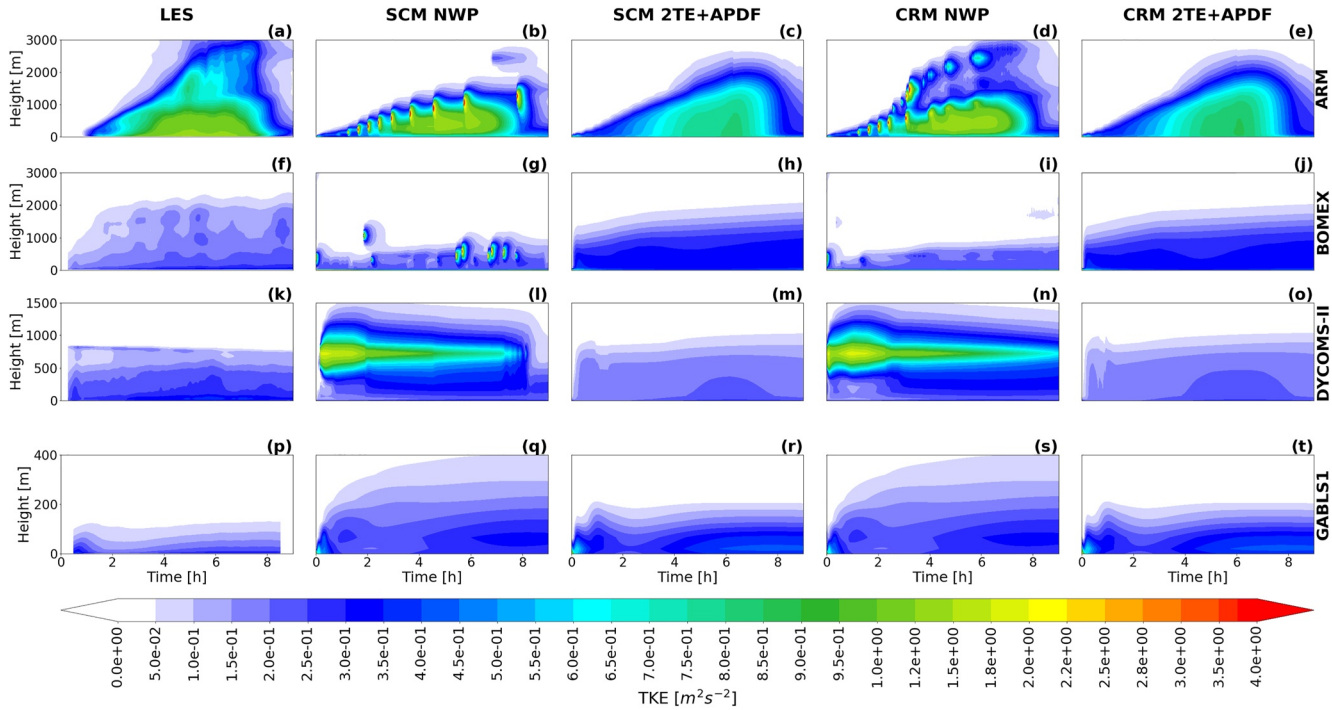

Figure 3. Evolution of the turbulence kinetic energy (TKE) for the same simulations as in Figure 2. Comparison between large eddy simulation (LES) (a, f, k, p), ICOsahedral Nonhydrostatic single column mode (ICON SCM) (b, g, l, q), and cloud resolving mode (CRM) (d, i, n, s) with operational setup, and ICON SCM (c, h, m, r) and CRM (e, j, o, t) with 2TE + APDF scheme.

scheme, where the top entrainment, which is strongly influenced by the turbulence length scale above the ABL top, should be small for stable and stratocumulus cases and should increase for shallow convection cases. In the second column, the comparison between the stability parameter used in the 2TE + APDF scheme, Ri_f^* (Equation 21 and the one used in the original 2TE scheme, Ri_f^{TE} (Equation 14), is also shown. Evidently, using Ri_f^{TE} results in a more intensive and deeper mixing than using the local stability parameter Ri_f^{GR} (Equation 22). As mentioned above, this leads to over-mixing in the original 2TE scheme, specifically for stratocumulus cases. The

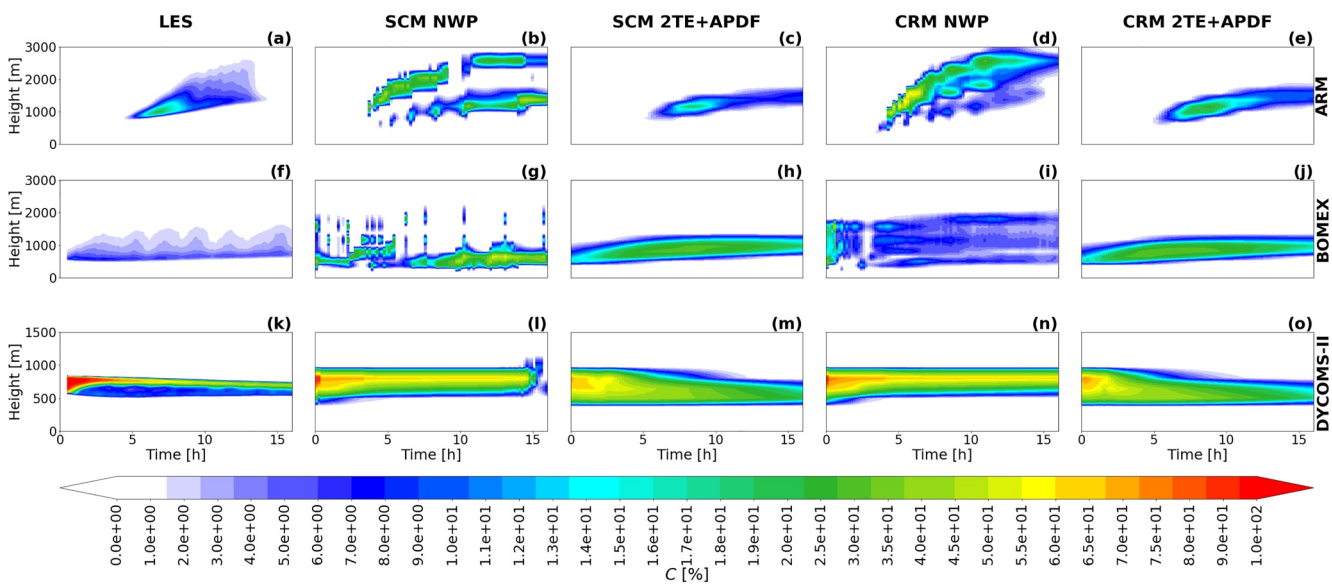

Figure 4. As in Figure 3, but evolution of the cloud fraction and without the GEWEX Atmospheric Boundary Layer Study (GABLS1) case.

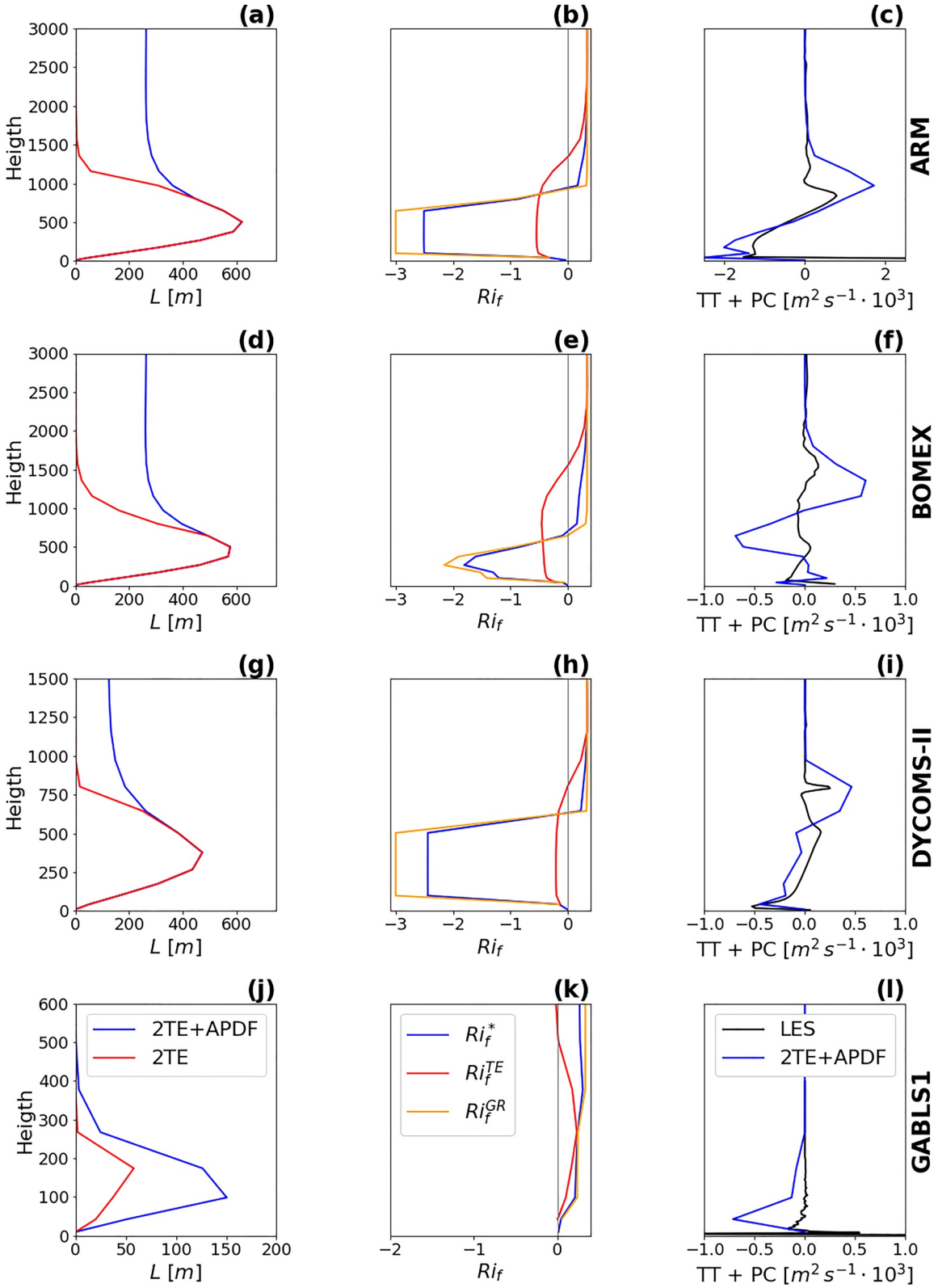
(a)
(b)
(c)
(d)
(e)
(f)
(g)
(h)
(i)
(j)
(k)
(l)
Heigth
L [m]
Ri_f
TT + PC [$m^2\,s^{-1}\cdot 10^3$]
ARM
BOMEX
DYCOMS-II
GABLS1
2TE+APDF
2TE
Ri_f^*
Ri_f^{TE}
Ri_f^{GR}
LES
2TE+APDF

Figure 5.

combined Ri_f^* still results in stronger mixing like for Ri_f^{TE}, which enables the scheme to parameterize shallow convection, but it is also influenced by local stratification. Third column shows the representation of the vertical turbulent transport and pressure correlation terms (see first term on the right hand side in Equation 9) in the 2TE + APDF scheme compared to the LES reference. While the magnitude of these terms tends to be too large (particularly for the BOMEX case), the shape of their vertical profiles resembles the profiles in the LES reference.

Please note that the computation of cloud fraction in the current simulations is not a part of the 2TE + APDF scheme, but an integral part of the NWP setup. Adjustment of the cloud fraction computation could also lead to an improvement of the 2TE + APDF scheme in this respect. For example, the internal cloud fraction obtained from the APDF method could contribute to the cloud fraction computation.

4. Real Case Simulations

Next, the 2TE + APDF scheme was tested on a real case to show that it can be used also in realistic three-dimensional simulations. For this purpose, we have chosen a case of summertime convection over land on the edge of a high pressure system from the observational Field Experiment on Submesoscale Spatio-Temporal VAriability in Lindenberg (see http://fesstval.de/) in eastern Germany 13 June 2021 starting at 00 UTC.

ICON was run in the limited area mode (LAM) for 24 hr with a time step of 10 s. Initial and lateral boundary conditions were taken from the operational weather forecast of the German Weather Service, ICON-EU, at 6.5 km horizontal resolution. The simulation was run in a 1-way nested configuration. The ICON LAM used a limited area grid over a circular domain with a radius of about 100 km centered at Falkenberg, Germany. The grid has 65 vertical levels and the horizontal grid spacing of about 2 km.

ICON in the large eddy mode (LEM; Bašták Ďurán et al., 2021; Dipankar et al., 2015; Heinze et al., 2017) was used as a reference. The ICON-LEM was run in a limited-area setup similar to ICON-LAM, but forced by the ICON-D2 operational forecasts and with an LEM physics setup (Dipankar et al., 2015). Please note that ICON-D2 is forced by ICON-EU. Four two-way nested grids with sequentially increasing horizontal resolution with about 600 m, 300 m, 150 m and 75 m were used. The four circular domains are centered around Falkenberg and cover an area with a radius of about 12 km for the inner-most grid. The time step was increased from 20 to 5 s with an increase in model resolution. Results were stored every 15 min.

Data computed on the second (DOM2) and the third (DOM3) ICON LEM domains were used for the evaluation of the ICON LAM results. The DOM3 data were used for evaluation of vertical profiles and height-time plots, where the ICON LEM statistics were calculated by averaging over 1 hr in time and over a rectangular region displayed in Figure 6. In order to obtain TKE that corresponds to the grid spacing of the ICON LAM a coarse graining method was used to compute TKE from ICON LEM data (see e.g., Bašták Ďurán et al., 2020; Honnert, 2016; Sakradzija et al., 2016; Zhang et al., 2018). The horizontal grid spacing of the coarsened rectangular domain (see Figure 6) roughly corresponds to the horizontal triangular grid spacing of the ICON LAM domain (grid areas are similar). For consistency, the ICON LAM data used in the vertical profiles and height-time plots were also obtained by horizontally averaging over the grid points inside the rectangular domain.

The horizontal and vertical cross sections of ICON LEM are displayed on DOM2 since it covers a larger region (see Figure 6).

Beside the NWP setup and 2TE + APDF scheme, the ICON model in the LAM was run also in an NWP setup with deactivated convection scheme (marked as NWP nC). This setup was run to verify the role of the convection scheme in the coupling between the turbulence scheme and the dynamics in the NWP setup.

Figure 7 shows the vertical profiles of the horizontal wind speed, the liquid water potential temperature, the total specific content of water, and the liquid water content, q_l, for ICON in the LEM and ICON in the LAM for

Figure 5. Vertical profiles of the turbulence length scales (a, d, g, j), the estimates of the flux Richardson number (b, e, h, k), and the sum of the turbulent transport (TT) and pressure correlation (PC) terms in the turbulence kinetic energy (TKE) equation (c, f, i, l) for the Atmospheric Radiation Measurement (ARM), Barbados Oceanographic and Meteorological Experiment (BOMEX), Dynamics and Chemistry of Marine Stratocumulus (DYCOMS-II), and GEWEX Atmospheric Boundary Layer Study (GABLS1) cases after 6 hr of integration in ICOsahedral Nonhydrostatic single column mode (ICON SCM) using the 2TE + APDF scheme. First column: comparison between 2TE + APDF length scale formulation (see Equation 26; blue) and the 2TE turbulence length scale formulation (see Equation 18; only diagnosed; red). Second column: comparison between Ri_f^* (see Equation 21; blue), Ri_f^{TE} (see Equation 14; red), and Ri_f^{GR} (see Equation 22; orange). Third column: comparison between large eddy simulation (LES; black) and ICON SCM (first term on the right hand side of Equation 9; blue).

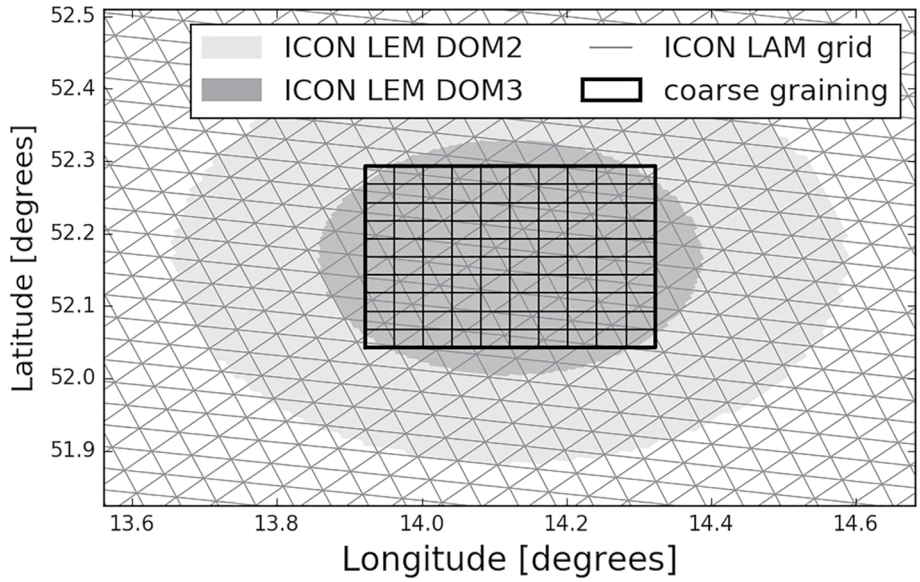

Figure 6. The second (DOM2—light gray shading) and third (DOM3—dark gray shading) horizontal domains used for the ICOsahedral Nonhydrostatic large eddy mode (ICON LEM) simulations. Triangular grid used for the ICON limited area mode (LAM) simulation is displayed with gray lines. The rectangular domain, on which the ICON LEM statistics are computed, is displayed with thick black lines. Thin black lines show the grid spacing of the coarsened grid that is used for the computation of turbulence kinetic energy (TKE) for ICON LEM.

the three configurations. The evolution of TKE is presented in Figure 8. Both plots confirm the results obtained for the idealized cases: the results for the 2TE + APDF scheme are more continuous in space and time, and the mixing is deeper for the NWP setup than for the 2TE + APDF scheme. The advantage of the mass-flux based convection scheme to mix also in a locally counter-gradient or non-gradient way is visible when it is compared with the NWP setup with deactivated convection. Namely, it is able to mimic ICON LEM in increasing vertical gradients of the liquid water potential temperature and the total specific content of water at the top of the ABL.

Horizontal cross-sections of the vertical velocity, the liquid water content and the surface turbulent heat fluxes for all configurations are compared to the ICON LEM in Figure 9. The 2TE + APDF scheme gives rise to elongated horizontal structures that resemble boundary-layer rolls that are very similar to the coherent flow structures produced by the ICON LEM at finer spatial scales. The resolved flow interacts (convergence and divergence) with these coherent structures and shows a good coupling between the 2TE + APDF scheme and the ICON

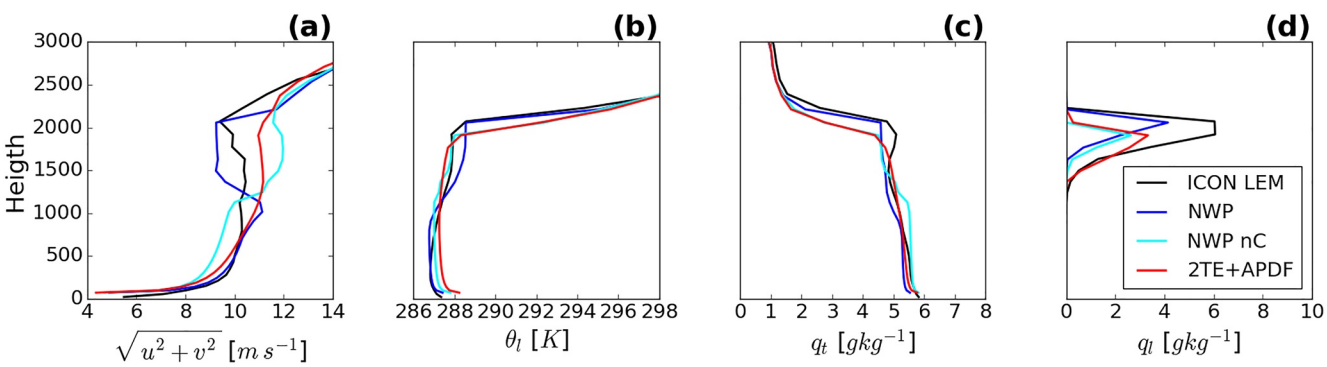

Figure 7. Vertical profiles of the horizontal wind speed (a), the liquid water potential temperature (b), the total specific content of water (c), and the liquid water content (d) for real case simulation over the Lindeberg Observatory starting on 13.06.2021 after 10 hr of integration, starting at 00 UTC. Comparison between ICOsahedral Nonhydrostatic large eddy mode (ICON LEM; black) and ICON limited area mode (LAM) with the NWP setup (blue), with the NWP setup with deactivated convection scheme (cyan), and with 2TE + APDF scheme (red).

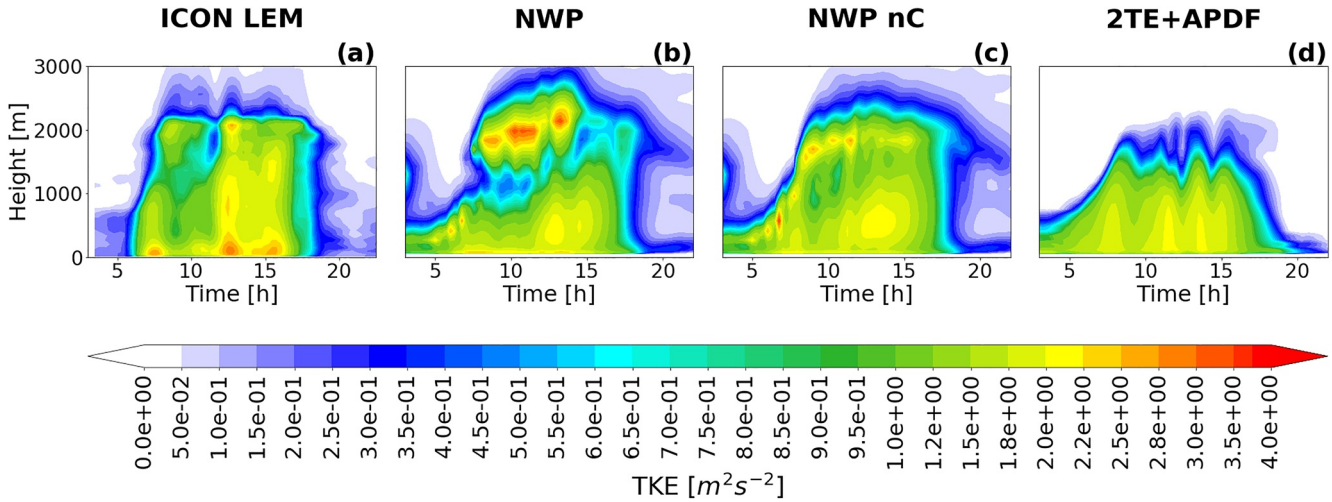

Figure 8. Evolution of the turbulence kinetic energy (TKE) for the same simulations as in Figure 7. Comparison between ICOsahedral Nonhydrostatic large eddy mode (ICON LEM) (a) and ICON limited area mode (LAM) with the NWP setup (b), with the NWP setup with deactivated convection scheme (c), and with 2TE + APDF scheme (d).

dynamical core. Clouds are formed at the top of the updraft flanks of the coherent roll structures (Figures 9e–9h) and imprint on the surface turbulent heat fluxes (Figures 9c, 9g, 9k, and 9o, 9m–9p and 9i–9l).

The NWP setup produces a different mode of organized resolved flow with structures that are oriented perpendicular to the horizontal wind direction and are less regular compared to the 2TE + APDF scheme. A striking feature of the NWP simulation is an undisturbed resolved horizontal flow that is decoupled from the coherent structures in the vertical velocity, the cloud field and the surface heat fluxes. This is also apparent from the evolution of the TKE in Figure 8. To locate the source of such model behavior in the NWP setup, we make a comparison with the NWP setup with deactivated convection scheme (Figures 9c, 9f, 9i, and 9l). The deactivation of convection in the latter simulation shows a decrease in coherency and regularity in the boundary layer compared to the NWP setup. This signifies that it is not sufficient to deactivate convection to achieve a better representation of the flow organization. The convection scheme actually increases the organization, but the character of the organization differs from the organization in the ICON LEM reference.

To get a more detailed view of the convective coherent structures that span across the depth of the boundary layer, we plotted also the vertical cross-sections of the vertical velocity and the liquid water content (Figure 10) along the horizontal line across the modeling domain indicated in Figure 9. The 2TE + APDF scheme produces roll structures that resemble those in ICON LEM in their spatial extent and strength, and a similar pattern in coupling to the clouds and ABL mixing. The NWP setups produce a weaker resolved flow and no apparent coherency in the ABL. Consequently, the cloud layer is more homogeneous compared to the ICON LEM and the 2TE + APDF scheme.

Based on the result from this real case, we can reiterate that the 2TE + APDF scheme can be used instead of a combination of the operational turbulence and convection scheme. While the later setup has the advantage of deeper and possible locally counter-gradient mixing, the APDF scheme has a more continuous behavior in time and space. This property is a direct consequence of using a pair of prognostic turbulence energies as the core control mechanism for turbulent mixing.

We assume that the usage of prognostic turbulence energies plays also a role in the good coupling between the 2TE + APDF scheme and the dynamics of the ICON model, which enables modeling of coherent flow structures in the ABL that resemble coherent structures in ICON LEM. The other factor in this coupling is that the 2TE + APDF scheme models the turbulence and convection in the ABL in a unified way. The inability of the NWP setup to model similar coherent flow structures is probably caused by inconsistencies, which are introduced by the separation of these processes.

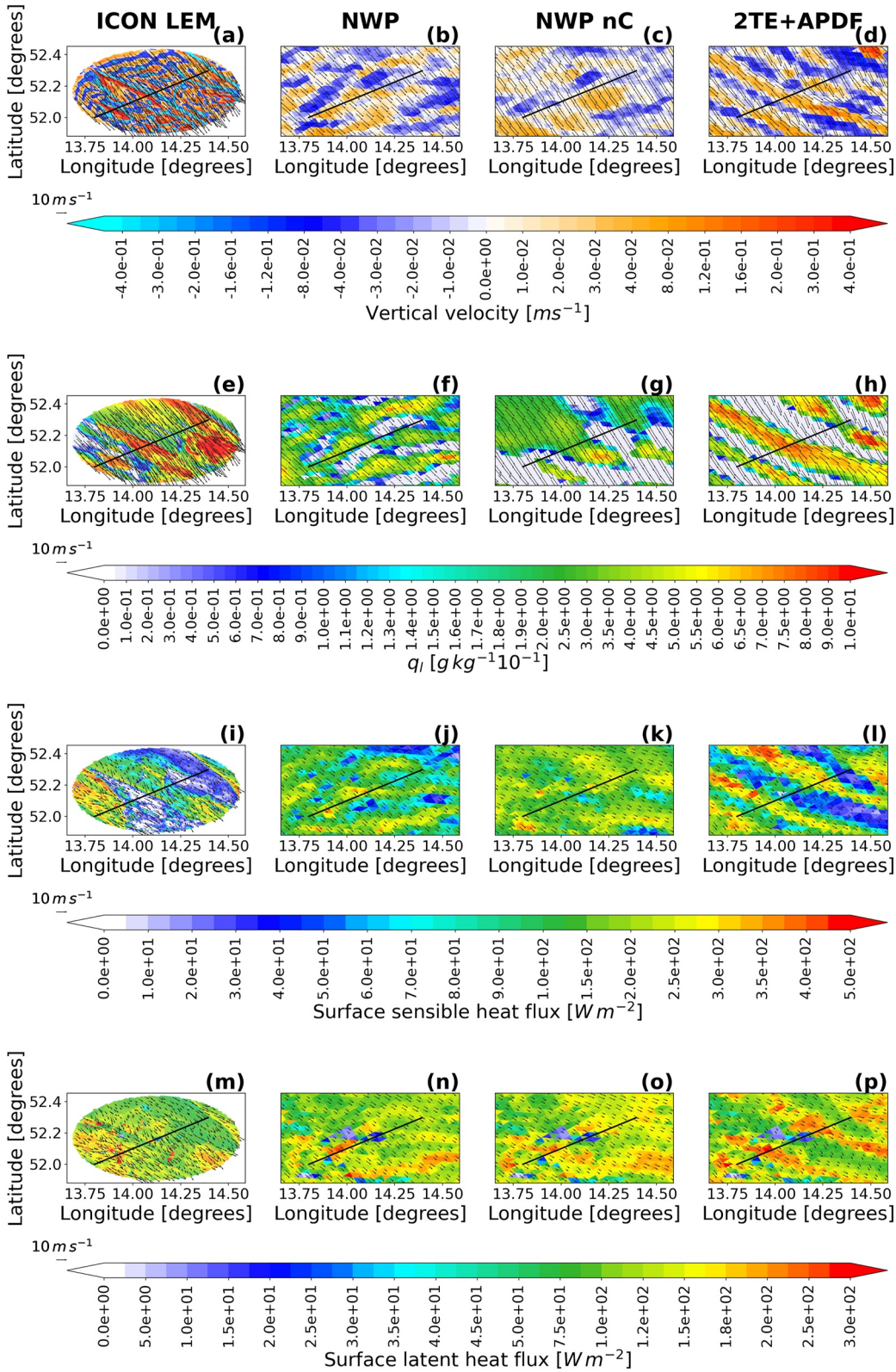

Figure 9. Horizontal cross sections of the vertical velocity (a–d) and the liquid water content (e–h) at the 44th model level height (approx. 1,900 m above the surface) and the latent heat flux (i–l) and the sensible heat flux (m–p) at the surface. Vector field of the horizontal velocity at the corresponding height is depicted with arrows. Black line indicates location of the vertical cross sections in Figure 10. Visualization of the same simulations as in Figure 7.

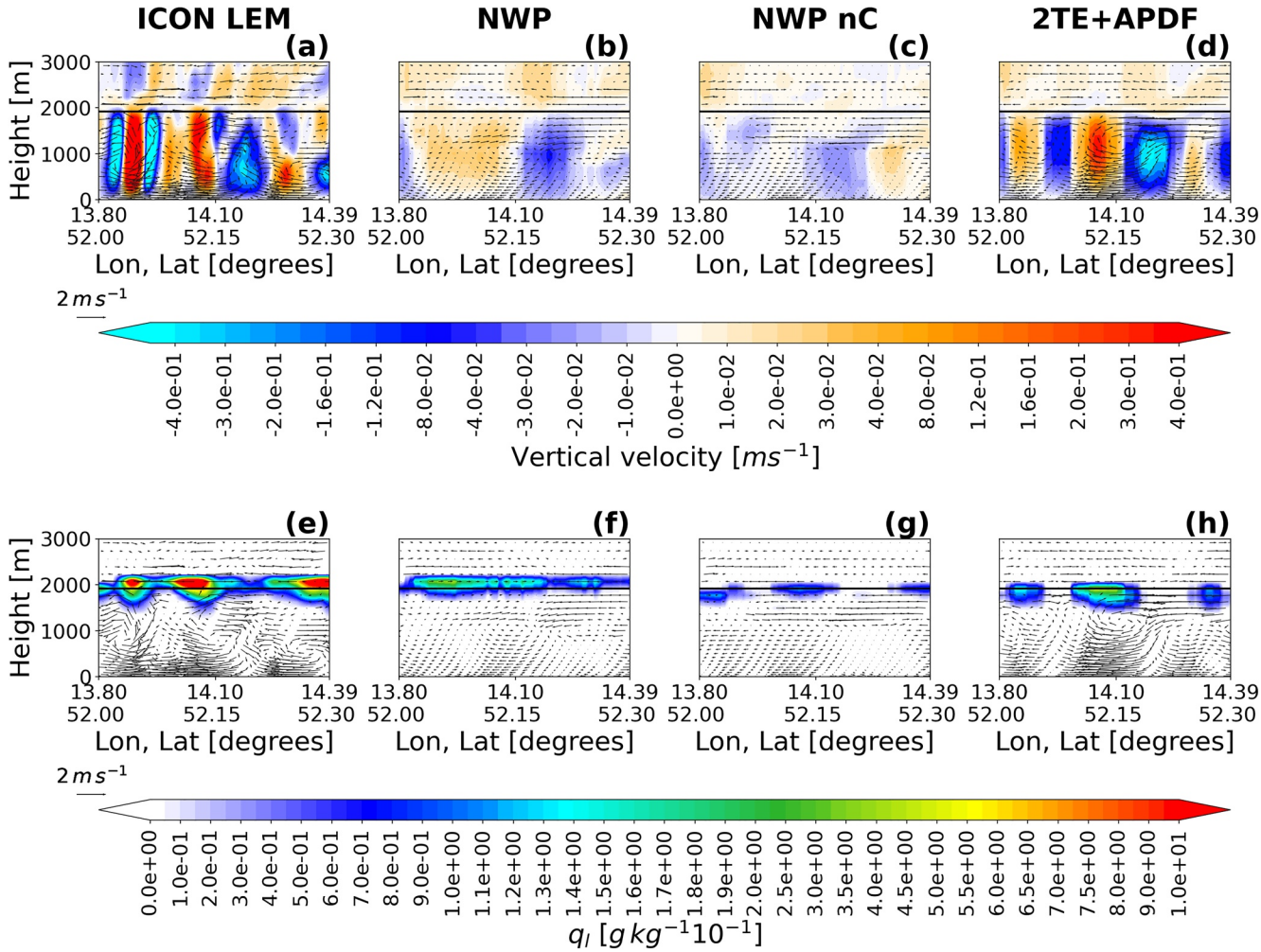

Figure 10. Vertical cross sections of the vertical velocity (a–d) and the liquid water content (e–h) along the cross section indicated by black line in Figure 9. Vector field of the along cross section relative (relative to domain mean) horizontal velocity and the vertical velocity is depicted with arrows. Black line indicates height of the horizontal cross sections in Figure 9. Visualization of the same simulations as in Figure 7.

We expect that the coupling between the 2TE + APDF scheme and the dynamics would be even further improved if the prognostic energies would be advected by the dynamics, which is currently not the case.

5. Summary and Conclusion

We have presented an update of the two-energy scheme (Bašták Ďurán et al., 2018). The original scheme suffered from a major deficiency: the overestimation of the erosion of stable layers due to overmixing, particularly in stratocumulus cases. We have identified the three causes for this problem: (a) the non-local stability parameter did not consider local stratification; (b) a lack of an internal parameter in the scheme that could distinguish between a shallow convection and a stratocumulus regime; and (c) an inflexible turbulence length scale formulation. All these causes are addressed in the update of the scheme by: (a) combining the non-local stability parameter with a local stability parameter; (b) using the turbulent flux and the bulk vertical gradient of the entropy potential temperature to distinguish between a shallow convection regime and a stratocumulus regime; and (c) an update of the turbulence length scale formulation. The original 2TE scheme was further coupled to the APDF method in order to achieve a more consistent and more universal representation of cloudy regimes. We coined the updated scheme as the 2TE + APDF scheme.

The updated turbulence scheme was evaluated for several idealized cases and one selected real case in the ICON modeling framework. There, the 2TE + APDF scheme was compared to the LES reference and the operational ICON model configuration, which consists of a prognostic TKE turbulence scheme (Cerenzia, 2017; Doms et al., 2013) and a mass-flux based convection scheme (Bechtold et al., 2008).

Compared to the original version of the scheme, the 2TE + APDF scheme is able to correct the overmixing at the top of the ABL in the stratocumulus case. The performance of the 2TE + APDF scheme is comparable to the operational ICON setup and can be thus used instead of combination of the operational turbulence and convection scheme in ICON. The ICON operational setup is able to mix faster and deeper and to maintain sharper gradients than the 2TE + APDF scheme, which can be sometimes beneficial. On the other hand, the 2TE + APDF scheme has a more continuous behavior in time and space. This feature is particularly important when looking at the evolution and the spatial structure of the ABL.

A demonstration of this fact is the ability of the 2TE + APDF scheme to model coherent flow structures in the ABL that resemble coherent structures in the LES for the selected real case. We assume that this is due to a better coupling between the 2TE + APDF scheme and the dynamics of the ICON model, which is due to the prognostic character of the 2TE + APDF scheme and its unified approach to modeling of turbulence and clouds in the ABL.

In the future, we plan to test the 2TE + APDF scheme thoroughly on several three-dimensional real cases and to investigate the capabilities of the 2TE + APDF scheme to model various coherent structures in the ABL. For this, the 2TE + APDF scheme will be extended to include the advection of the prognostic energies. We also plan to utilize the internal cloud fraction based on the APDF for a better estimation of the cloud fraction.

Data Availability Statement

The data for this study were generated with the large eddy simulation model MicroHH, which are openly available in Zenodo at https://zenodo.org/record/822842 (C. C. van Heerwaarden et al., 2017). The configuration files, outputs, and visualization scripts for the ICOsahedral Nonhydrostatic (ICON) simulations are openly available in Zenodo at: https://doi.org/10.5281/zenodo.6403030 (Bašták Ďurán et al., 2022). The code of the 2TE + APDF scheme in ICON, together with the configuration for the idealized cases and the python scripts for the generation of the forcing can be accessed after registration at the internal DWD GitLab repository (https://gitlab.dkrz.de/) in the icon-nwp/icon-nwp-scm-2te + apdf branch. All figures were generated with the Python matplotlib package (Hunter, 2007). This project took advantage of netCDF software developed by UCAR/Unidata (http://doi.org/10.5065/D6H70CW6).

Acknowledgments
The authors thanks Ján Mašek from the CHMI, who helped to shape this paper with the discussion on the stability parameter. The authors thank also Daniel Klocke and Linda Schlemmer for their assistance in setting up of the ICON LEM. This research was funded by the Hans Ertel Centre for Weather Research of DWD (third phase, The Atmospheric Boundary Layer in Numerical Weather Prediction) Grant No. 4818DWDP4; and the Deutsche Forschungsgemeinschaft (DFG, German Research Foundation)—TRR 301—Project-ID 428312742. This work used resources of the Deutsches Klimarechenzentrum (DKRZ) granted by its Scientific Steering Committee (WLA) under project ID bb1096. Open access funding enabled and organized by Projekt DEAL.

References

Bašták Ďurán, I., Geleyn, J.-F., & Váňa, F. (2014). A compact model for the stability dependency of TKE production-destruction-conversion terms valid for the whole range of Richardson numbers. *Journal of the Atmospheric Sciences*, *71*(8), 3004–3026. https://doi.org/10.1175/JAS-D-13-0203.1

Bašták Ďurán, I., Geleyn, J.-F., Váňa, F., Schmidli, J., & Brožková, R. (2018). A turbulence scheme with two prognostic turbulence energies. *Journal of the Atmospheric Sciences*, *75*(10), 3381–3402. https://doi.org/10.1175/JAS-D-18-0026.1

Bašták Ďurán, I., Köhler, M., Eichhorn-Müller, A., Maurer, V., Schmidli, J., Schomburg, A., et al. (2021). The ICON single-column mode. *Atmosphere*, *12*(7), 906. https://doi.org/10.3390/atmos12070906

Bašták Ďurán, I., Sakradzija, M., & Schmidli, J. (2022). *Data accompanying the paper titled: The two-energies turbulence scheme coupled to the assumed PDF method*. Zenodo. https://doi.org/10.5281/zenodo.6403030

Bašták Ďurán, I., Schmidli, J., & Bhattacharya, R. (2020). A budget-based turbulence length scale diagnostic. *Atmosphere*, *11*(4), 425. https://doi.org/10.3390/atmos11040425

Beare, R. J., Macvean, M. K., Holtslag, A. A. M., Cuxart, J., Esau, I., Golaz, J.-C., et al. (2006). An intercomparison of large-eddy simulations of the stable boundary layer. *Boundary-Layer Meteorology*, *118*(2), 247–272. https://doi.org/10.1007/s10546-004-2820-6

Bechtold, P., Bazile, E., Guichard, F., Mascart, P., & Richard, E. (2001). A mass-flux convection scheme for regional and global models. *Quarterly Journal of the Royal Meteorological Society*, *127*(573), 869–886. https://doi.org/10.1002/qj.49712757309

Bechtold, P., Köhler, M., Jung, T., Doblas-Reyes, F., Leutbecher, M., Rodwell, M. J., et al. (2008). Advances in simulating atmospheric variability with the ECMWF model: From synoptic to decadal time-scales. *Quarterly Journal of the Royal Meteorological Society*, *134*(634), 1337–1351. https://doi.org/10.1002/qj.289

Bechtold, P., Semane, N., Lopez, P., Chaboureau, J.-P., Beljaars, A., & Bormann, N. (2014). Representing equilibrium and nonequilibrium convection in large-scale models. *Journal of the Atmospheric Sciences*, *71*(2), 734–753. https://doi.org/10.1175/JAS-D-13-0163.1

Bogenschutz, P. A., & Krueger, S. K. (2013). A simplified PDF parameterization of subgrid-scale clouds and turbulence for cloud-resolving models. *Journal of Advances in Modeling Earth Systems*, *5*(2), 195–211. https://doi.org/10.1002/jame.20018

Bougeault, P. (1981). Modeling the trade-wind cumulus boundary layer. Part II: A high-order one-dimensional model. *Journal of the Atmospheric Sciences*, *38*(11), 2429–2439. https://doi.org/10.1175/1520-0469(1981)038<2429:MTTWCB>2.0.CO;2

Bougeault, P., & Lacarrere, P. (1989). Parameterization of orography-induced turbulence in a mesobeta–scale model. *Monthly Weather Review*, *117*(8), 1872–1890. https://doi.org/10.1175/1520-0493(1989)117<1872:POOITI>2.0.CO;2

Bretherton, C. S., & Park, S. (2009). A new moist turbulence parameterization in the community atmosphere model. *Journal of Climate*, *22*(12), 3422–3448. https://doi.org/10.1175/2008JCLI2556.1

Brown, A. R., Cederwall, R. T., Chlond, A., Duynkerke, P. G., Golaz, J.-C., Khairoutdinov, M., et al. (2002). Large-eddy simulation of the diurnal cycle of shallow cumulus convection over land. *Quarterly Journal of the Royal Meteorological Society*, *128*(582), 1075–1093. https://doi.org/10.1256/003590002320373210

Canuto, V., Cheng, Y., & Howard, A. (2007). Non-local ocean mixing model and a new plume model for deep convection. *Ocean Modelling*, *16*(1), 28–46. https://doi.org/10.1016/j.ocemod.2006.07.003

Cedilnik, J. (2005). *Parallel suites documentation*. LACE Report. Retrieved from http://www.rclace.eu/File/Physics/2005/cedilnik_stay_2005.pdf

Cerenzia, I. (2017). Challenges and critical aspects in stable boundary layer representation in numerical weather prediction modeling: Diagnostic analyses and proposals for improvement (Unpublished doctoral dissertation). *Alma Mater Studiorum Universita di Bologna*discussion. https://doi.org/10.6092/unibo/amsdottorato/8067

Cheng, Y., Canuto, V., & Howard, A. (2002). An improved model for the turbulent PBL. *Journal of the Atmospheric Sciences*, *59*(9), 1550–1565. https://doi.org/10.1175/1520-0469(2002)059<1550:AIMFTT>2.0.CO;2

Crueger, T., Giorgetta, M. A., Brokopf, R., Esch, M., Fiedler, S., Hohenegger, C., et al. (2018). ICON-A, the atmosphere component of the ICON Earth system model: II. Model evaluation. *Journal of Advances in Modeling Earth Systems*, *10*(7), 1638–1662. https://doi.org/10.1029/2017MS001233

Cuxart, J., Bougeault, P., & Redelsperger, J.-L. (2000). A turbulence scheme allowing for mesoscale and large-eddy simulations. *Quarterly Journal of the Royal Meteorological Society*, *126*(562), 1–30. https://doi.org/10.1002/qj.49712656202

Cuxart, J., Holtslag, A. A. M., Beare, R. J., Bazile, E., Beljaars, A., Cheng, A., et al. (2006). Single-column model intercomparison for a stably stratified atmospheric boundary layer. *Boundary-Layer Meteorology*, *118*(2), 273–303. https://doi.org/10.1007/s10546-005-3780-1

Deardorff, J. W. (1972). Theoretical expression for the countergradient vertical heat flux. *Journal of Geophysical Research*, *77*(30), 5900–5904. https://doi.org/10.1029/JC077i030p05900

Dipankar, A., Stevens, B., Heinze, R., Moseley, C., Zängl, G., Giorgetta, M., & Brdar, S. (2015). Large eddy simulation using the general circulation model ICON. *Journal of Advances in Modeling Earth Systems*, *7*(3), 963–986. https://doi.org/10.1002/2015MS000431

Doms, G., Förstner, J., Heise, E., Herzog, H.-J., Mironov, D., Raschendorfer, M., et al. (2013). *A description of the nonhydrostatic regional COSMO-model. Part II – Physical parameterizations*. DWD. Retrieved from http://www.cosmo-model.org/content/model/documentation/core/cosmo_physics_5.00.pdf

Doms, G., Förstner, J., Heise, E., Herzog, H.-J., Mironov, D., Raschendorfer, M., et al. (2018). *A description of the nonhydrostatic regional COSMO-model, part II, physical parameterizations*. COSMO Technical Documentation. Retrieved from http://www.cosmomodel.org/content/model/documentation/core/cosmo_physics_5.05.pdf

Giorgetta, M. A., Brokopf, R., Crueger, T., Esch, M., Fiedler, S., Helmert, J., et al. (2018). ICON-A, the atmosphere component of the ICON Earth system model: I. Model description. *Journal of Advances in Modeling Earth Systems*, *10*(7), 1613–1637. https://doi.org/10.1029/2017MS001242

Golaz, J.-C., Larson, V. E., & Cotton, W. R. (2002). A PDF-based model for boundary layer clouds. Part I: Method and model description. *Journal of the Atmospheric Sciences*, *59*(24), 3540–3551. https://doi.org/10.1175/1520-0469(2002)059<3540:APBMFB>2.0.CO;2

Heinze, R., Dipankar, A., Henken, C. C., Moseley, C., Sourdeval, O., Trömel, S., et al. (2017). Large-eddy simulations over Germany using ICON: A comprehensive evaluation. *Quarterly Journal of the Royal Meteorological Society*, *143*(702), 69–100. https://doi.org/10.1002/qj.2947

Holtslag, A. A. M., & Moeng, C.-H. (1991). Eddy diffusivity and countergradient transport in the convective atmospheric boundary layer. *Journal of the Atmospheric Sciences*, *48*(14), 1690–1698. https://doi.org/10.1175/1520-0469(1991)048<1690:EDACTI>2.0.CO;2

Holtslag, B. (2006). Preface: GEWEX atmospheric boundary-layer study (GABLS) on stable boundary layers. *Boundary-Layer Meteorology*, *118*(2), 243–246. https://doi.org/10.1007/s10546-005-9008-6

Honnert, R. (2016). Representation of the grey zone of turbulence in the atmospheric boundary layer. *Advances in Science and Research*, *13*, 63–67. https://doi.org/10.5194/asr-13-63-2016

Hunter, J. D. (2007). Matplotlib: A 2D graphics environment. *Computing in Science & Engineering*, *9*(3), 90–95. https://doi.org/10.1109/MCSE.2007.55

Janjic, Z. (2002). Nonsingular implementation of the Mellor–Yamada level 2.5 scheme in the NCEP Meso model. *NCEP Office Note, 436*.

Krueger, S. K. (1988). Numerical simulation of tropical cumulus clouds and their interaction with the subcloud layer. *Journal of the Atmospheric Sciences*, *45*(16), 2221–2250. https://doi.org/10.1175/1520-0469(1988)045<2221:NSOTCC>2.0.CO;2

Larson, V., Schanen, D., Wang, M., Ovchinnikov, M., & Ghan, S. (2012). PDF parameterization of boundary layer clouds in models with horizontal grid spacings from 2 to 16 km. *Monthly Weather Review*, *140*(1), 285–306. https://doi.org/10.1175/MWR-D-10-05059.1

Larson, V. E., Golaz, J.-C., & Cotton, W. R. (2002). Small-scale and mesoscale variability in cloudy boundary layers: Joint probability density functions. *Journal of the Atmospheric Sciences*, *59*(24), 3519–3539. https://doi.org/10.1175/1520-0469(2002)059<3519:SSAMVI>2.0.CO;2

Lenderink, G., Siebesma, A. P., Cheinet, S., Irons, S., Jones, C. G., Marquet, P., et al. (2004). The diurnal cycle of shallow cumulus clouds over land: A single-column model intercomparison study. *Quarterly Journal of the Royal Meteorological Society*, *130*(604), 3339–3364. https://doi.org/10.1256/qj.03.122

Machulskaya, E., & Mironov, D. V. (2013). *Implementation of TKE-scalar variance mixing scheme into COSMO*. COSMO Newsletter, No. 13. Retrieved from http://www.cosmo-model.org/content/model/documentation/newsLetters/newsLetter13/cnl13_03.pdf

Marquet, P. (2011). Definition of a moist entropy potential temperature: Application to FIRE-I data flights. *Quarterly Journal of the Royal Meteorological Society*, *137*(656), 768–791. https://doi.org/10.1002/qj.787

Marquet, P., & Bechtold, P. (2020). In E. Astakhova (Ed.), *A new Estimated Inversion Strength (EIS) based on the moist-air entropy. Research activities in Earth system modelling. Working Group on Numerical Experimentation* (Report No50. WCRP Report No12/2020. No. 50). WMO. http://bluebook.meteoinfo.ru/uploads/2020/docs/04_Marquet_Pascal_NewEntropyEIS.pdf

Marquet, P., & Geleyn, J.-F. (2013). On a general definition of the squared Brunt-Väisälä frequency associated with the specific moist entropy potential temperature. *Quarterly Journal of the Royal Meteorological Society*, *139*(670), 85–100. https://doi.org/10.1002/qj.1957

Marquet, P., & Stevens, B. (2021). On moist potential temperatures and their ability to characterize differences in the properties of air parcels. *Journal of the Atmospheric Sciences*, *79*(4), 1089–1103. https://doi.org/10.1175/JAS-D-21-0095.1

Nakanishi, M., & Niino, H. (2009). Development of an improved turbulence closure model for the atmospheric boundary layer. *Journal of the Meteorological Society of Japan. Series II*, *87*(5), 895–912. https://doi.org/10.2151/jmsj.87.895

Neggers, R. A. J. (2009). A dual mass flux framework for boundary layer convection. Part II: Clouds. *Journal of the Atmospheric Sciences*, *66*(6), 1489–1506. https://doi.org/10.1175/2008JAS2636.1

Neggers, R. A. J., Köhler, M., & Beljaars, A. C. M. (2009). A dual mass flux framework for boundary layer convection. Part I: Transport. *Journal of the Atmospheric Sciences*, *66*(6), 1465–1487. https://doi.org/10.1175/2008JAS2635.1

Sakradzija, M., Seifert, A., & Dipankar, A. (2016). A stochastic scale-aware parameterization of shallow cumulus convection across the convective gray zone. *Journal of Advances in Modeling Earth Systems*, *8*(2), 786–812. https://doi.org/10.1002/2016MS000634

Sakradzija, M., Senf, F., Scheck, L., Ahlgrimm, M., & Klocke, D. (2020). Local impact of stochastic shallow convection on clouds and precipitation in the tropical Atlantic. *Monthly Weather Review*, *148*(12), 5041–5062. https://doi.org/10.1175/MWR-D-20-0107.1

Siebesma, A. P., Bretherton, C. S., Brown, A., Chlond, A., Cuxart, J., Duynkerke, P. G., et al. (2003). A large eddy simulation intercomparison study of shallow cumulus convection. *Journal of the Atmospheric Sciences*, *60*(10), 1201–1219. https://doi.org/10.1175/1520-0469(2003)60<1201:ALESIS>2.0.CO;2

Siebesma, A. P., Soares, P. M. M., & Teixeira, J. (2007). A combined eddy-diffusivity mass-flux approach for the convective boundary layer. *Journal of the Atmospheric Sciences*, *64*(4), 1230–1248. https://doi.org/10.1175/JAS3888.1

Sommeria, G., & Deardorff, J. W. (1977). Subgrid-scale condensation in models of nonprecipitating clouds. *Journal of the Atmospheric Sciences*, *34*(2), 344–355. https://doi.org/10.1175/1520-0469(1977)034<0344:SSCIMO>2.0.CO;2

Stevens, B., Moeng, C.-H., Ackerman, A. S., Bretherton, C. S., Chlond, A., de Roode, S., et al. (2005). Evaluation of large-eddy simulations via observations of nocturnal marine stratocumulus. *Monthly Weather Review*, *133*(6), 1443–1462. https://doi.org/10.1175/MWR2930.1

Sušelj, K., Teixeira, J., & Matheou, G. (2012). Eddy diffusivity/mass flux and shallow cumulus boundary layer: An updraft PDF multiple mass flux scheme. *Journal of the Atmospheric Sciences*, *69*(5), 1513–1533. https://doi.org/10.1175/JAS-D-11-090.1

Termonia, P., Fischer, C., Bazile, E., Bouyssel, F., Brožková, R., Bénard, P., et al. (2018). The ALADIN system and its canonical model configurations AROME CY41T1 and ALARO CY40T1. *Geoscientific Model Development*, *11*(1), 257–281. https://doi.org/10.5194/gmd-11-257-2018

Tiedtke, M. (1989). A comprehensive mass flux scheme for cumulus parameterization in large-scale models. *Monthly Weather Review*, *117*(8), 1779–1800. https://doi.org/10.1175/1520-0493(1989)117<1779:ACMFSF>2.0.CO;2

van Heerwaarden, C., van Stratum, B., & Heus, T. (2017). *microhh/microhh: 1.0.0*. Zenodo. https://doi.org/10.5281/zenodo.822842

van Heerwaarden, C. C., van Stratum, B. J. H., Heus, T., Gibbs, J. A., Fedorovich, E., & Mellado, J. P. (2017). MicroHH 1.0: A computational fluid dynamics code for direct numerical simulation and large-eddy simulation of atmospheric boundary layer flows. *Geoscientific Model Development*, *10*(8), 3145–3165. https://doi.org/10.5194/gmd-10-3145-2017

Wang, Y., Belluš, M., Ehrlich, A., Mile, M., Pristov, N., Smolíková, P., et al. (2018). 27 years of regional cooperation for limited area modelling in central Europe (RC LACE). *Bulletin of the American Meteorological Society*, *99*(7), 1415–1432. https://doi.org/10.1175/BAMS-D-16-0321.1

Zängl, G., Reinert, D., Rípodas, P., & Baldauf, M. (2015). The ICON (ICOsahedral Non-hydrostatic) modelling framework of DWD and MPI-M: Description of the non-hydrostatic dynamical core. *Quarterly Journal of the Royal Meteorological Society*, *141*(687), 563–579. https://doi.org/10.1002/qj.2378

Zängl, G., & Schäfer, S. (2021). *Model configuration upgrade of icon*. DWD. Retrieved from https://www.dwd.de/DE/fachnutzer/forschung_lehre/numerische_wettervorhersage/nwv_aenderungen/_functions/DownloadBox_modellaenderungen/icon/pdf_2021/pdf_icon_14_04_2021.pdf

Zhang, X., Bao, J.-W., Chen, B., & Grell, E. D. (2018). A three-dimensional scale-adaptive turbulent kinetic energy scheme in the wrf-arw model. *Monthly Weather Review*, *146*(7), 2023–2045. https://doi.org/10.1175/MWR-D-17-0356.1

Zilitinkevich, S., Elperin, T., Kleeorin, N., Rogachevskii, I., & Esau, I. (2013). A hierarchy of energy- and flux-budget (EFB) turbulence closure models for stably-stratified geophysical flows. *Boundary-Layer Meteorology*, *146*(3), 341–373. https://doi.org/10.1007/s10546-012-9768-8

Zilitinkevich, S., Elperin, T., Kleeorin, N., Rogachevskii, I., Esau, I., Mauritsen, T., & Miles, M. W. (2008). Turbulence energetics in stably stratified geophysical flows: Strong and weak mixing regimes. *Quarterly Journal of the Royal Meteorological Society*, *134*(633), 793–799. https://doi.org/10.1002/qj.264

Zilitinkevich, S. S., Elperin, T., Kleeorin, N., & Rogachevskii, I. (2007). Energy- and flux-budget (EFB) turbulence closure model for stably stratified flows. Part I: Steady-state, homogeneous regimes. *Boundary-Layer Meteorology*, *125*(2), 167–191. https://doi.org/10.1007/s10546-007-9189-2